Theor Chem Acc (2011) 130:739–748
DOI 10.1007/s00214-011-0914-z

REGULAR ARTICLE

Singlet–triplet energy gap for trimethylenemethane, oxyallyl diradical, and related species: single- and multireference computational results

Toru Saito · Satomichi Nishihara · Shusuke Yamanaka · Yasutaka Kitagawa · Takashi Kawakami · Satoru Yamada · Hiroshi Isobe · Mitsutaka Okumura · Kizashi Yamaguchi

Received: 24 December 2010 / Accepted: 23 February 2011 / Published online: 10 March 2011

Abstract We have investigated the through-bond exchange interactions in three non-Kekulé hydrocarbon diradicals on the basis of single- and multireference coupled cluster and related broken-symmetry (BS) methods. The singlet–triplet energy gap (S-T gap) and diradical characters for these species are evaluated. It is found that the spin contamination involved in the BS solutions is non-negligible and the approximate spin-projection method greatly improves the usual BS solutions. As for Mukherjee's state-specific multireference coupled cluster (MkMRCC) computations, the size-consistent correction with the UHF localized natural orbitals (ULO) is useful to obtain the qualitatively correct $2J$ values.

Keywords Multireference coupled cluster · Spin-projection method · Broken-symmetry method · Diradical species

Dedicated to Professor Akira Imamura on the occasion of his 77th birthday and published as part of the Imamura Festschrift Issue.

Electronic supplementary material The online version of this article (doi:10.1007/s00214-011-0914-z) contains supplementary material, which is available to authorized users.

T. Saito (✉) · S. Nishihara · S. Yamanaka · Y. Kitagawa · T. Kawakami · S. Yamada · H. Isobe · M. Okumura
Department of Chemistry, Graduate School of Science, Osaka University, 1-1 Machikaneyama, Toyonaka, Osaka 560-0043, Japan
e-mail: tsaito@chem.sci.osaka-u.ac.jp

K. Yamaguchi
NanoScience Design Center, Osaka University, 1-3 Machikaneyama, Toyonaka, Osaka 560-8531, Japan

1 Introduction

The singlet and triplet energy separations in diradical species have attracted great attention in relation to possible reaction mechanisms [1, 2]. Trimethylenemethane (TMM) and oxyallyl (OXA) diradicals have been widely investigated by both experimental and theoretical approaches [3–25]. TMM is a typical example of non-Kekulé hydrocarbon diradical, and electron paramagnetic resonance (EPR) spectroscopy confirmed its ground state to be the triplet. The adiabatic S($^1A_1$)-T($^3A_2'$) gap of $\sim$16.1 kcal/mol was determined by photoelectron spectroscopic measurements [8]. OXA can be viewed as a derivative of TMM, where a methylene group is replaced by an oxygen atom. For organic reactions, OXA is considered to be a transition state or a diradical intermediate in the rearrangement of allene oxide to cyclopropanone, in the ring opening of cyclopropanone, in the Favorskii rearrangement, and so on [4, 11, 14, 18]. In contrast to TMM, the highest occupied molecular orbital (MO) (HOMO) ($2b_1$) and lowest unoccupied MO (LUMO) ($1a_2$) of OXA are not exactly degenerate due to the oxygen substitution. Although the S-T gap of OXA predicted by early and recent theoretical calculations varied among methods [5, 6, 21, 22, 25], the rigorous assignment of the ground state had not been achieved because there was no experimental data for comparison. Very recently, however, Ichino et al. revealed that the ground state is $^1A_1$, but the adiabatic energy of the $^3B_2$ state is only (55 $\pm$ 2) meV (1.3 kcal/mol) higher than that of the singlet ground state [22].

Since the strong electron correlation effects in π-conjugated organic radicals should be considered, first-principle calculations with high accuracy beyond the "gold-standard" coupled cluster (CC) singles and doubles with

perturbative triples excitations (CCSD(T)) are required [26, 27]. It is well known that the single-reference spin-restricted Hartree–Fock (RHF)-based approach provides a poor description of such degenerate or near-degenerate systems [28]. The post-RHF methods even RCCSD(T) do not improve the zeroth-order RHF wave function. Instead, broken-symmetry (BS) and multireference (MR) methods have been utilized for these systems. The perturbation theory based on the complete active space self-consistent field (CASSCF) wave function such as MRMP2 [29] and CASPT2 [30] can describe both the nondynamical and dynamical correlation effects at a reasonable computational cost. However, in some cases, calculated results heavily depend on the active space. For example, the barrier height of $^1O_2 + C_2H_4$ reaction differs by the selected active space. The barrier height calculated at the CASPT2 (10e,10o) level was 17.5 kcal/mol [31], while that calculated at the MRMP2(12e,12o) level was 6.1 kcal/mol [32]. Note that (12e,12o) represents 12 electrons in 12 orbitals. The intruder state problem involved in the MR-based perturbation theories can also affect this difference [33]. Therefore, more rigorous approaches including the genuine multireference coupled cluster (MRCC) theories are desirable to deal with (quasi-)degenerate systems. Recently, many types of MRCC have been formulated and implemented by several groups [34–40]. Among various types of MRCC, the state-specific MRCC, which is size-extensive and intruder free, is a promising approach to overcome these problems.

Although the BS methods can treat nondynamical correlation effects with low computational cost as compared to the MR methods, they involve spin contamination, which then has to be treated [41, 42]. We have examined the spin contamination effect quantitatively by using an approximate spin-projection (AP) method [43–45]. To assess the applicability of AP-BS approaches for diradical systems, we took Mukherjee's state-specific multireference coupled cluster singles and doubles (MkMRCCSD) method as a reference [37, 40]. The results of the spin-unrestricted Hartree–Fock (UHF)-based coupled cluster singles and doubles (UCCSD) method and those of the coupled cluster doubles based on the spin-unrestricted Brueckner orbital (UBD) method [46, 47] after the AP correction (AP-UCCSD and AP-UBD) were in good agreement with the MkMRCCSD results [48–51]. In the present study, we focus on the validity of AP-BS methods to through-bond ferromagnetic coupling as well as anti-ferromagnetic coupling in π-conjugated organic systems as follows: (1) TMM, (2) iminoallyl (IA), and (3) OXA. Thus, systematic comparisons between BS methods with MkMRCCSD are performed based on the singlet–triplet energy gaps ($2J$) and diradical character of (1)–(3).

2 Theoretical backgrounds

2.1 Approximate spin-projection method

The effective exchange interactions between local spins can be described by using the Heisenberg spin Hamiltonian. In the case of two spin systems, it is defined as

$$H_{\text{Heisenberg}} = -2J\mathbf{S}_1 \cdot \mathbf{S}_2, \tag{1}$$

where $\mathbf{S}_1$ and $\mathbf{S}_2$ are spin operators for each site and J represents an effective exchange integral. According to Yamaguchi and his co-workers [43–45], the effective exchange integral (J) is given as follows:

$$J = \frac{E^{\text{LS}} - E^{\text{HS}}}{\left\langle \hat{\mathbf{S}}^2 \right\rangle^{\text{HS}} - \left\langle \hat{\mathbf{S}}^2 \right\rangle^{\text{LS}}}, \tag{2}$$

where LS and HS mean, respectively, the low-spin and high-spin states. E and $<\mathbf{S}^2>$ denote the total energy and total spin angular momentum, respectively. The exact $<\mathbf{S}^2>^{\text{LS}}$ value is zero in the case of the singlet ($S = 0$) state. When using the BS methods, however, the $<\mathbf{S}^2>^{\text{LS}}$ value is not always equal to the corresponding exact value. The $<\mathbf{S}^2>^{\text{LS}}$ value is often considered as a measure of spin contamination involved in the BS solutions. The extrapolation with Eq. 2 yields the approximate total energy of the pure LS state as

$$E^{\text{AP}} = E^{\text{LS}} - J\left(S_z^{\text{LS}}(S_z^{\text{LS}} + 1) - \left\langle \mathbf{S}^2 \right\rangle^{\text{LS}}\right). \tag{3}$$

In this way, the approximate spin-projection (AP) method removes the spin contamination from UHF-based methods and UDFT methods.

The $<\mathbf{S}^2>^{\text{LS}}$ values of the post-UHF methods are assumed as

$$\left\langle \mathbf{S}^2 \right\rangle_X = \frac{\langle \Psi_X | \mathbf{S}^2 | \Psi_X \rangle}{\langle \Psi_X | \Psi_X \rangle}, \tag{4}$$

where X denotes UCCSD, UBD, and so on. The evaluation of Eq. 4 involves very high computational cost. In this study, we adopted the practical scheme proposed by Purvis et al. [52], where $\left\langle \mathbf{S}^2 \right\rangle_{\text{UCC}}$ is assumed as

$$\left\langle \mathbf{S}^2 \right\rangle_X \approx \frac{\langle \Psi_{\text{UHF}} | \mathbf{S}^2 | \Psi_X \rangle}{\langle \Psi_{\text{UHF}} | \Psi_X \rangle}. \tag{5}$$

The Eq. 5 is also employed for the UBD method.

2.2 Estimation of diradical character and effective bond order

To obtain symmetry-adapted picture from the BS solutions, the natural orbitals are defined as eigenfunctions of the first-order density matrices [53]

$$\rho(\mathbf{r};\mathbf{r}') = \sum n_i \{\phi_i(\mathbf{r})\}^* \phi_i(\mathbf{r}'), \tag{6}$$

where n_i denotes the natural orbital occupation numbers (NOON). NOONs of bonding and anti-bonding natural orbitals are almost 2.0 and 0.0, respectively. ψ_i^+ and ψ_i^- represent the BS MOs.

$$|\psi_i^{\pm}\rangle = \cos\theta_i |\phi_i^b\rangle \pm \sin\theta_i |\phi_i^a\rangle. \tag{7}$$

θ is the mixing parameter between the symmetry-adapted bonding $|\phi_i^b\rangle$ and anti-bonding $|\phi_i^a\rangle$ orbitals. The corresponding NOONs (n_i^+ and n_i^-) are given by the orbital overlap S_i between the corresponding orbital pairs.

$$n_i^{\pm} = 1 \pm S_i, \tag{8}$$

where

$$S_i = \langle \psi_i^+ \mid \psi_i^- \rangle = \cos 2\theta. \tag{9}$$

The diradical character is given by the weight of the doubly excited configuration W_D in CI terminology, and it is expressed by

$$Y_i = 2W_D = 1 - \frac{2S_i}{1+S_i^2}. \tag{10a}$$

For diradical systems, i corresponds to the highest occupied natural orbital (HONO)–lowest unoccupied natural orbital (LUNO) pair. The effective bond order B_i is also introduced to express the reduction in bond order by using diradical character

$$B_i = 1 - Y_i = \frac{2S_i}{1+S_i^2} \tag{10b}$$

In the case of the smallest active space (2e,2o), four reference configurations are applied to MkMRCCSD calculations.

$$\begin{aligned}
|\Phi_1\rangle &= \left|(\text{core})^{2n}(\text{inactive})^{2m} x\bar{x}\right\rangle, \\
|\Phi_2\rangle &= \left|(\text{core})^{2n}(\text{inactive})^{2m} y\bar{y}\right\rangle, \\
|\Phi_3\rangle &= \left|(\text{core})^{2n}(\text{inactive})^{2m} x\bar{y}\right\rangle, \\
|\Phi_4\rangle &= \left|(\text{core})^{2n}(\text{inactive})^{2m} y\bar{x}\right\rangle,
\end{aligned} \tag{11}$$

where n and m represent the number of the doubly occupied frozen-core and inactive orbitals, respectively. The term (x, y) is the (HOMO, LUMO) pair. The singlet and triplet states of the MkMRCCSD wave functions are described by

$$|\Psi_S\rangle = c_1 e^{T_1}|\Phi_1\rangle + c_2 e^{T_2}|\Phi_2\rangle \quad (c_1 \geq c_2) \tag{12}$$

and

$$|\Psi_T\rangle = \frac{1}{\sqrt{2}}\left(e^{T_3}|\Phi_3\rangle - e^{T_4}|\Phi_4\rangle\right), \tag{13}$$

respectively. Note that Eq. 12 is correct only if the HOMO and LUMO belong to the different irreps such that the contribution of the open-shell singlet configurations ($|\Phi_3\rangle, |\Phi_4\rangle$) is excluded. The CI coefficient c and amplitude T are determined via an iterative procedure. Therefore, the diradical character (Y) can be defined using the coefficients c in Eq. 12 of the ground and doubly excited configurations as follows:

$$Y = 2c_2^2 \tag{14}$$

The MkMRCCSD is designed to satisfy the size-extensive condition, but it does not satisfy the size-consistent condition, which is critical to investigate the bond dissociation problems [40]. In addition to the delocalized active orbitals, we also used localized ones. The localized active orbitals can be obtained from the symmetry-adapted bonding $|\phi^b\rangle$ and anti-bonding $|\phi^a\rangle$ orbitals as

$$|\psi^{\pm}\rangle = \frac{1}{\sqrt{2}}|\phi^b\rangle \pm \frac{1}{\sqrt{2}}|\phi^a\rangle. \tag{15}$$

3 Computational details

Figure 1 illustrates computational schemes for diradical (or polyradical) species starting from the BS calculations: (1) semi-canonical spin-restricted open-shell HF (ROHF) orbital, (2) CASSCF natural orbital (CNO), (3) UHF natural orbital (UNO), and localized ones of (1)–(3), namely, RLO, CLO, and ULO. The computational methods in Fig. 1 are applied to elucidate electronic and spin states of the following diradical species: TMM, IA, and OXA as illustrated in Fig. 2. Full geometry optimizations were performed at the UCAM-B3LYP level [54]. The geometry optimizations were employed in the singlet (BS) and triplet (HS) states. For single-point energy calculations, the cc-pVDZ basis sets [55] were used unless otherwise noted. The UBLYP, UB3LYP, UBHandHLYP, ULC-BLYP, and UCAM-B3LYP methods were employed as the UDFT computations [54, 56–59]. The parameters of Coulomb

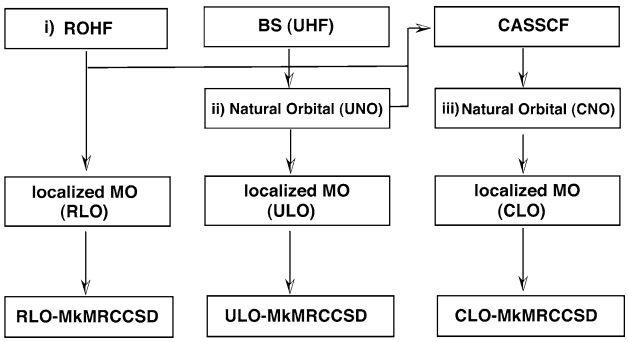

Fig. 1 Computational scheme for MkMRCCSD computations

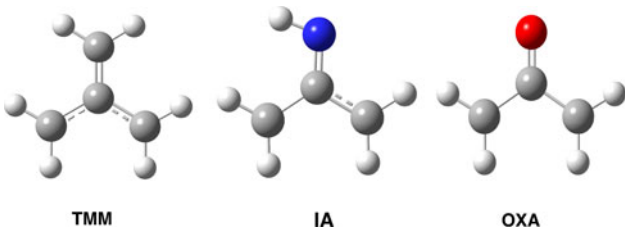

Fig. 2 Calculated diradical species: TMM, IA, and OXA

division scheme were $\mu = 0.47$ for LC-BLYP functional, and $\mu = 0.33$, $\alpha = 0.19$, $\alpha + \beta = 0.65$ for CAM-B3LYP functional, respectively. The UHF, UCCSD, UCCSD(T), UBD, and UBD(T) methods [27, 46, 47] were also performed for single-point energy calculations. The BS (e.g., UHF and UDFT) calculations were performed by Gaussian09 program package [60], which was modified to calculate $\langle \mathbf{S}^2 \rangle_X$ values in the Eq. 5. The CASSCF calculations were performed by GAMESS program package [61], and MkMRCCSD calculations were performed by PSI3 program package [62], which was modified to use the initial orbitals.

4 Results and discussions

4.1 Trimethylenemethane

The optimized geometries are provided in the Supporting Information. The obtained $<S^2>$ values are summarized in Table 1. The adiabatic S-T gap ($2J$) determined by the energy difference between E^{AP} at the BS optimized geometry and E^{HS} at the HS optimized geometry. It must be noted that the $2J$ value used hereafter in this paper differs from the vertical $2J$ value defined by Eqs. 1–3. The $2J$ values for TMM, IA, and OXA calculated by the present and previous single-reference methods with the experimental data are summarized in Table 2. The corresponding results calculated by the present and previous MR methods with the experimental data are summarized in Table 3. The calculated Y values are summarized in Table 4.

Figure 3 shows two singly occupied MOs (SOMOs) for TMM, IA, and OXA obtained at the ROHF/cc-pVDZ level together with the orbital energies of the two SOMOs in the parentheses. As shown in Fig. 3, the energies of non-bonding HOMO-LUMO pair are exactly degenerate, and the obtained $<S^2>^{LS}$ and Y values support it. The $<S^2>^{LS}$ value often plays an important role in measuring the degree of the spin contamination effect. The dynamical electron correlation corrections for the UHF solution such as UCCSD rather enhance the $<S^2>^{LS}$ values, while the $<S^2>^{LS}$ values obtained by UDFT methods are close to 1.0. This can be attributed to the fact that post-UHF methods stabilize the BS solutions by increasing the spin contamination when the HS state is the ground state as in the case of CH_2 [48]. The use of spin-unrestricted Brueckner orbital, in which the contribution of single excitations is set to zero, also provides the $<S^2>^{LS}$ value similar to the UCCSD result. The $<S^2>^{HS}$ value calculated by

Table 1 Total spin angular momentums $<\mathbf{S}^2>$ values for trimethylenemethane (TMM), iminoallyl (IA), and oxyallyl (OXA) by the broken-symmetry (BS) methods

Method	TMM		IA		OXA	
	LS	HS	LS	HS	LS	HS
UHF	1.0198	2.1932	1.0722	2.1965	0.9710	2.1778
UCCSD	1.1107	2.0278	1.0575	2.0269	0.9331	2.0218
UBLYP	1.0037	2.0173	0.9444	2.0160	0.7547	2.0120
UB3LYP	1.0051	2.0334	0.9643	2.0324	0.8363	2.0249
UCAM-B3LYP	1.0078	2.0697	0.9821	2.0709	0.9031	2.0579
UBHandHLYP	1.0056	2.0490	0.9755	2.0463	0.8824	2.0342
ULC-BLYP	1.0060	2.0722	0.9842	2.0656	0.9203	2.0443
UBD	1.1293	2.0132	1.0609	2.0117	0.9195	2.0082

Table 2 The $2J$ values (kcal/mol) for trimethylenemethane (TMM), iminoallyl (IA), and oxyallyl (OXA) calculated by the single-reference methods

Method	TMM	IA	OXA
AP-UHF	44.3	39.6	22.3
AP-UCCSD	25.0	18.3	4.7
AP-UCCSD(T)	17.9	13.5	1.8
AP-UBD	26.1	18.3	4.9
AP-UBD(T)	18.3	13.3	2.2
AP-UBLYP	15.8	9.5	−3.5
AP-UB3LYP	21.6	15.2	1.2
AP-UCAM-B3LYP	25.6	18.4	3.9
AP-UBHandHLYP	29.6	23.5	8.4
AP-ULC-BLYP	30.4	21.2	5.7
RMRCCSD/cc-pVTZ[a]	23.8		
SS-EOM-CCSD[+2][b]	19.8		
EOM-SF-CC(2,3)/cc-pVTZ[c]	18.2		
EOM-SF-CCSD(dT)/aug-cc-pVTZ[d]			−1.5
Expt.	16.1[e]		−1.3[f]

The results with the use of the cc-pVDZ basis sets are presented unless otherwise noted

[a] Ref. [20]

[b] Ref. [19]

[c] Ref. [16]

[d] Ref. [25]

[e] Ref. [8]

[f] Ref. [22]

Table 3 The 2*J* values (kcal/mol) for trimethylenemethane (TMM), iminoallyl (IA), and oxyallyl (OXA) calculated by the MR methods

Method	TMM	IA	OXA
CASSCF(2e,2o)	11.6	4.3	−5.2
ROHF-MkMRCCSD(2e,2o)	20.6	14.6	1.6
CNO-MkMRCCSD(2e,2o)	21.0	13.0	1.5
UNO-MkMRCCSD(2e,2o)	21.3	13.5	1.7
RLO-MkMRCCSD(2e,2o)	20.0	12.2	−0.2
CLO-MkMRCCSD(2e,2o)	14.9	8.2	−2.3
ULO-MkMRCCSD(2e,2o)	15.8	9.1	−1.6
4R BWCCSD it/cc-pVTZ[a]	17.8		
CASPT2(12e,11o)[b]		12.7 (12.0)	
CASPT2(2e,2o)/6-31G*[c]			3.4
CASPT2(4e,4o)/6-31G*[c]			3.1
CASPT2(4e,4o)/aug-cc-pVTZ[d]			−0.4
CASPT2(6e,5o)[e]			1.6
MRCISD(2e,2o)/6-31G*[c]			−1.5
MRCISD(4e,4o)/6-31G*[c]			3.2
MR-ACPF(6e,5o)/cc-pVTZ[e]			0.3
Expt.	16.1[f]		−1.3[d]

The results with the use of the cc-pVDZ basis sets are presented unless otherwise noted

[a] Ref. [17]

[b] Ref. [10]. Values in the parenthesis represent the results together with the cc-pVTZ basis sets

[c] Ref. [21]

[d] Ref. [22]

[e] Ref. [11]

[f] Ref. [8]

Table 4 The *Y* values (%) for trimethylenemethane (TMM), iminoallyl (IA), and oxyallyl (OXA) by the BS (Eq. 10a is used) and MR (Eq. 14 is used) methods

Method	TMM	IA	OXA
AP-UHF	98.9	78.2	58.6
AP-UBD[a]	98.9	77.0	48.3
AP-UBLYP	99.7	53.9	20.1
AP-UB3LYP	99.4	61.1	29.7
AP-UCAM-B3LYP	99.2	66.2	37.6
AP-UBHandHLYP	99.1	68.6	41.6
AP-ULC-BLYP	99.5	71.1	46.2
CASSCF(2e,2o)	97.1	71.3	52.9
ROHF-MkMRCCSD(2e,2o)	97.9	–[b]	46.5
CNO-MkMRCCSD(2e,2o)	98.5	68.9	46.3
UNO-MkMRCCSD(2e,2o)	98.4	70.0	45.5

The corresponding effective bond order *B* (%) is give by 100-*Y*

[a] The *Y* values are calculated in the Fermi vacuum

[b] The *Y* value is not defined

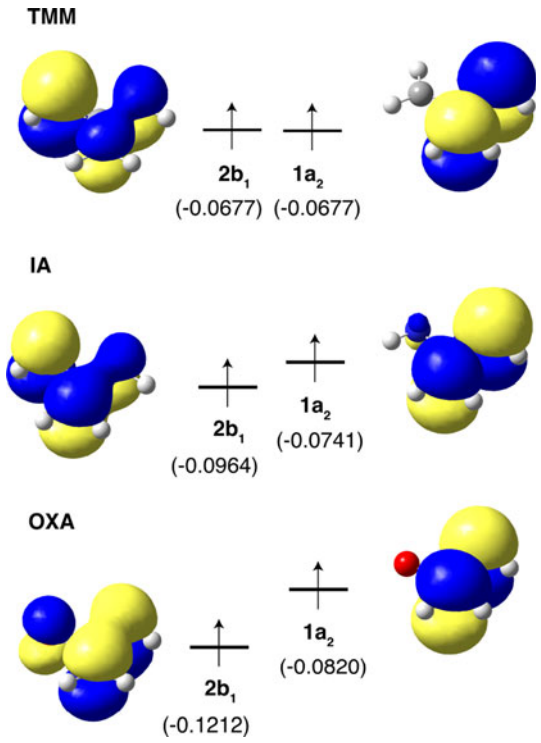

Fig. 3 Two singly occupied MOs (SOMOs) of TMM, IA, and OXA obtained at the ROHF/cc-pVDZ level. Values in *parentheses* represent the orbital energies of the two SOMOs

UHF is slightly larger than the exact value. This deviation is caused by the spin polarization of the (HOMO − 1)-(LUMO + 1) pair in the UHF solution. The $<S^2>^{HS}$ values decrease with increasing the dynamical correlation effects in accordance with the behavior of the UDFT results.

The 2*J* value for TMM has been predicted to be positive at many different levels of theory. Since the spin polarization effect in the HS state is large at the UHF level, the calculated 2*J* value significantly overestimates the experimental value by 28 kcal/mol. The inclusion of the dynamical electron correlation corrections improves the 2*J* value. As listed in Table 2, the AP-UCCSD and AP-UBD methods with the cc-pVDZ basis sets yield results similar to the reduced multireference coupled cluster with singles and doubles (RMRCCSD) with multiconfigurational SCF (MCSCF) MOs result with the cc-pVTZ basis sets (23.8 kcal/mol) [20]. The perturbative triple excitation corrections (T) decrease the 2*J* value by ∼8 kcal/mol. These results become comparable to the state-specific equation-of-motion CCSD (SS-EOM-CCSD[+2]) with the cc-pVDZ basis sets (19.8 kcal/mol) [19] and equation-of-motion spin-flip CC (EOM-SF-CC(2,3)) with the cc-pVTZ basis sets (18.2 kcal/mol) [16]. As for the AP-UDFT results, the calculated 2*J* value heavily depends on the XC functional, especially the HF exchange ratio. The magnitude of the 2*J* value increases in the following order:

AP-UBLYP < AP-UB3LYP < AP-UCAM-B3LYP < AP-UBHandHLYP < AP-ULC-BLYP. According to the experimental value, the AP-UBLYP method, which does not contain HF exchange term, outperforms the global hybrid and range-separated hybrid methods.

The CASSCF(2e,2o) method, which is free from the spin contamination effect, provides the smaller 2*J* value than the AP-UHF method as summarized in Table 3. The CC exponential ansatz in the MkMRCCSD theory greatly changes the CASSCF(2e,2o) result. The choice of the reference orbitals for MkMRCCSD calculation does not effect on the S-T gap of TMM. The differences in the 2*J* values among the three reference orbitals are within 0.7 kcal/mol. On the other hand, the RMRCCSD or state-universal CCSD (SU CCSD) results can vary with reference orbitals [63]. In fact, the RMRCCSD energy differences between MCSCF MOs and RHF MOs reach at most 6.8 kcal/mol [20]. In this way, the MkMRCCSD method with the delocalized active orbitals is less sensitive to the types of reference orbitals. However, the MkMRCCSD results with localized active orbitals change the situation. The ULO- and CLO-MkMRCCSD methods reduce the 2*J* value more than 5 kcal/mol from the results with the delocalized active orbitals, while the RLO-MkMRCCSD method involves a relatively small change (1.3 kcal/mol). It suggests that the choice of reference orbitals is important when using the localized active orbitals. On the basis of the MkMRCCSD and experimental results, the AP-UCCSD(T), AP-UBD(T), and AP-UBLYP methods perform well for the S-T gap of TMM.

4.2 Iminoallyl

Iminoallyl (IA) can be viewed as a derivative of TMM, where a methylene group is replaced by the NH group. In 1998, Cramer and his co-workers first investigated the aza analogs of TMM including IA [10]. The calculated 2*J* value was 12.7 (12.0) kcal/mol at the CASPT2(12e,11o)/cc-pVDZ (cc-pVTZ) level as summarized in Table 3. They suggested that the replacement of CH_2 by NH group might stabilize the singlet state relative to the triplet state by about 7 kcal/mol. In other words, the best estimate of 2*J* value for IA is about 9 kcal/mol. The $<S^2>^{LS}$ values for IA are smaller than those for TMM except for UHF, whereas there is not much difference in $<S^2>^{HS}$ value between TMM and IA. The HOMO ($2b_1$) and LUMO ($1a_2$) are not perfectly degenerate due to the NH substitution as shown in Fig. 3. The obtained *Y* values range from 53.9 to 78.2%, supporting this behavior.

The relation between the 2*J* values and calculated methods of IA is almost similar to that of TMM. The AP-UHF method seems to overestimate the 2*J* value, while the AP-UCCSD and AP-UBD stabilize the BS state with respect to the HS state. The results of AP-UCCSD(T) and AP-UBD(T) are in good agreement with those of CASPT2(12e,11o). In the case of UDFT, the calculated 2*J* value systematically increases with increasing HF exchange ratio for the pure and global hybrid XC functionals in the following order: UBLYP < UB3LYP < UBHandHLYP. Unlike TMM, AP-UCAM-B3LYP and AP-ULC-BLYP yield smaller 2*J* values as compared to AP-UBHandHLYP. The difference in the 2*J* value between CASSCF(2e,2o) and MkMRCCSD is ~10 kcal/mol as in the case of TMM. The obtained ROHF-MkMRCCSD wave function includes the $|\Phi_3\rangle$ and $|\Phi_4\rangle$ configurations with coefficient 0.21 because IA has an asymmetric structure. Therefore, the diradical character based on the ROHF-MkMRCCSD solution cannot be defined correctly (see Sect. 2.2). The unstable ROHF-MkMRCCSD solution causes the overestimation of the 2*J* value by more than 1 kcal/mol in comparison with the CNO- and UNO-MkMRCCSD results. This trend is more remarkable when using the localized active orbitals. Both the CLO- and ULO-MkMRCCSD methods reproduce the best estimate value of ~9 kcal/mol, whereas the RLO-MkMRCCSD method does not remedy the 2*J* value. From the results, the ROHF can be less reliable than UNO and CNO for TMM and IA. Also, the AP-UBLYP method is comparable to the MkMRCCSD calculations with the size-consistent correction.

4.3 Oxyallyl

As described above, many questions with respect to OXA had remained unsolved until the detection of the singlet ($^1A_1$) and triplet ($^3B_2$) states by using negative ion photoelectron spectroscopy [22]. The answers to the important questions are as follows: The singlet state is the ground state. OXA is not a local minimum on the potential energy surface and undergoes barrierless ring-closure to form cyclopropanone. The sophisticated EOM-SF-CCSD(dT) calculations performed by Krylov et al. were in good agreement with the experimental facts [25], while many theoretical methods have tended to provide the triplet ground state [5, 6, 11, 21]. Here, we would like to investigate the scope and applicability of the MkMRCC and AP-BS approaches on the 2*J* value for OXA.

In contrast to TMM and IA, the differences in the $<S^2>^{LS}$ and *Y* values between calculated methods are notable. The 2*J* value calculated at the AP-UBLYP level qualitatively agrees with the experiment in accordance with TMM and IA. On the other hand, the other single-reference methods even AP-UCCSD(T) in combination with the cc-pVDZ basis sets predict that the triplet state is the ground state, although the magnitude of the 2*J* value decreases with increasing the electron correlation. The CASSCF(2e,2o) calculation gives the singlet ground state,

but it can be due to the fact that it overstabilizes the singlet state, judging from the results of TMM and IA. The MkMRCCSD calculations with the delocalized active orbitals also give the positive $2J$ values as in the case of the most AP-BS methods. The sign of the $2J$ value changes with the use of the localized active orbitals. The ULO-MkMRCCSD result agrees with the multireference configuration interaction method with all singles and doubles (MRCISD) with the (2e,2o) active space [21] and EOM-SF-CCSD(dT) results [25] as well as the experiment (see Table 3). Hence, the MkMRCCSD(2e,2o) computations with the size-consistent correction should be imperative to reproduce the qualitative $2J$ values for OXA qualitatively.

However, the computations with larger active space including $1b_1$ and $3b_1$ orbitals show a confused behavior. As listed in Table 3, the MRCISD(4e,4o) and more rigorous MR averaged coupled-pair functional (MR-ACPF) with the (6e,5o) active space computations predicted the triplet ground state with the positive $2J$ values of 3.2 and 0.3 kcal/mol, respectively [11, 21]. These results are qualitatively consistent with the CASPT2(4e,4o)/6-31G(d) result performed by Shen et al., while the CASPT2(4e,4o)/aug-cc-pVTZ calculation performed by Ichino et al. confirmed the singlet ground state. This discrepancy suggests that the active space and basis sets used for the single-point energy calculations can affect the sign of $2J$ value because the CASSCF geometry optimizations were performed in both the cases. For this reason, we performed additional CASSCF and MRMP2 calculations in combination with the cc-pVDZ and cc-pVTZ basis sets. To check the basis set dependency strictly, natural orbitals obtained by the spin-unrestricted quadratic configuration interaction singles and doubles (UQCISD) method were used for the reference orbitals as shown in Fig. 4.

The (HONO − 1)-(LUNO + 1) pair, which appears in the (4e,4o) active space, is just the same as the conventional one adopted consciously. Note that it is determined automatically if the NOONs of post-UHF methods are used. The calculations with the active spaces consisting of (HONO − X)-(LUNO + X) pairs ($X = 0, 1, 2,...$) up to $X = 5$ (i.e., (12e,12o)) were employed in a black box manner (instead of using experience to choose them). All active orbitals used in the present study are depicted in Fig. S1 in the Supporting Information. Table 5 summarizes the $2J$ values obtained by the CASSCF and MRMP2 methods. The UCCSD and UCCSD(T) calculations were also employed by using larger aug-cc-pVDZ, *d*-aug-cc-pVDZ, cc-pVTZ, aug-cc-pVTZ *d*-aug-cc-pVTZ, and cc-pVQZ basis sets [64]. The $2J$ values calculated by the AP-UCCSD and AP-UCCSD(T) methods are summarized in Table 6.

As listed in Table 5, at the cc-pVDZ level, CASSCF (6e,6o) gives the singlet ground state in accord with CASSCF(2e,2o), but larger active spaces settle into the triplet ground state with small positive $2J$ values. The singlet state seems to be overstabilized at the CASSCF(6e,6o) level and the subsequent the MRMP2(6e,6o) calculations yield large positive $2J$ value, which is significantly different from the other results. None of the MRMP2 calculations reproduce the singlet ground state with the use of the cc-pVDZ basis sets. In contrast to the cc-pVDZ basis sets, the cc-pVTZ basis sets together with

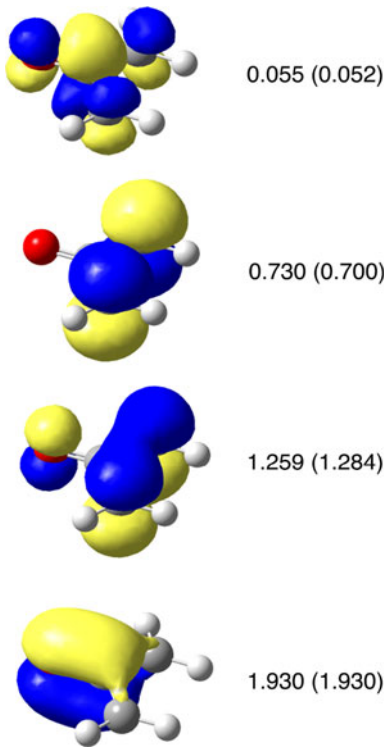

Fig. 4 The natural orbitals of the (4e,4o) active space with their occupation numbers obtained at the UQCISD/cc-pVDZ (cc-pVTZ) level

Table 5 The $2J$ values (kcal/mol) for OXA at the CASSCF(Xe, Xo) and MRMP2(Xe, Xo) ($X = 2, 4, 6, 8, 10, 12$) levels with the cc-pVDZ and cc-pVTZ basis sets

Method	Active space	cc-pVDZ	cc-pVTZ
CASSCF	(2e,2o)	−3.7	−6.3
	(4e,4o)	5.1	3.8
	(6e,6o)	−6.1	−7.5
	(8e,8o)	0.3	−0.9
	(10e,10o)	0.6	−0.7
	(12e,12o)	0.6	−1.2
MRMP2	(2e,2o)	2.2	1.9
	(4e,4o)	2.6	1.4
	(6e,6o)	5.6	4.5
	(8e,8o)	2.9	1.9
	(10e,10o)	2.8	1.9
	(12e,12o)	2.2	−0.1

Table 6 The 2*J* values (kcal/mol) for OXA at the AP-UCCSD and AP-UCCSD(T) levels with the aug-cc-pVDZ, *d*-aug-cc-pVDZ, cc-pVTZ, aug-cc-pVTZ, *d*-aug-cc-pVTZ, and cc-pVQZ basis sets

Basis sets	Method	
	AP-UCCSD	AP-UCCSD(T)
aug-cc-pVDZ	2.5	−0.3
d-aug-cc-pVDZ	2.6	0.3
cc-pVTZ	2.8	0.2
aug-cc-pVTZ	2.1	−0.5
d-aug-cc-pVTZ	2.2	−0.5
cc-pVQZ	2.0	−0.6

CAS sizes larger than (6e,6o) give the negative 2*J* values. Nevertheless, the MRMP2 calculation shows negative 2*J* values only with the (12e,12o) active space. Thus, it is quite difficult to choose an appropriate active space for OXA if it is greater than (2e,2o). It is found that adding only the (HONO − 1)-(LUNO + 1) pair to the HONO-LUNO pair seems to be insufficient for the prediction of the 2*J* value for OXA appropriately. On the other hand, the AP-UCCSD and AP-UCCSD(T) methods represent the decrease in the 2*J* values with increasing basis set size. Table 6 shows that a larger basis set, probably of at least aug-cc-pVTZ quality is needed to exhibit the singlet ground state within a single-reference framework. At the aug-cc-pVTZ level, the AP-UCCSD(T) result is qualitatively consistent with EOM-SF-CCSD(dT) result despite the fact that the former slightly underperforms the latter on the basis of the experimental value.

5 Conclusions

In this study, we have performed systematic comparisons of MkMRCCSD and BS methods focusing on the through-bond interactions of TMM and related species based on the S-T gaps (2*J*) and diradical characters. The spin contamination effect involved in the BS solutions is non-negligible, and it arises mainly from the triplet state. The AP method with the use of the approximate $<S^2>$ value for post-HF methods greatly improves the usual BS solutions. In the case of TMM and IA, the AP-UCCSD(T), AP-UBD(T), and AP-UBLYP results perform well concerning the adiabatic S-T gap on the basis of MR methods. The sign of the 2*J* value for OXA is sensitive to the CAS size since the singlet and triplet states are nearly degenerate in energy. However, the best choice of the active space is unclear. To avoid the dependency of the active space, the minimal active space based on the UNO should be rigorous without requiring chemical intuition. Then, the dynamical electron correlation effects should be considered by highly accurate CC methods including UNO-MkMRCCSD. As for MkMRCC computations, it is found that the size-consistent correction with the localized active orbitals is requisite to obtain the qualitatively correct 2*J* values, although the calculated results can depend on the reference orbitals. Judging from the calculated results, the UNO-based ULO as well as CNO-based CLO is more reliable than the ROHF-based RLO. In fact, the ULO-MkMRCCSD(2e,2o) calculation predicts the singlet ground state. When the AP-BS methods are performed, the combination with high-level *ab inito* methods with large and flexible basis sets is imperative. The AP-BS methods together with cc-pVDZ basis sets do not reproduce the singlet ground state of OXA except for AP-UBLYP, while the AP-UCCSD(T)/aug-cc-pVTZ calculation qualitatively reproduces the EOM-SF-CCSD(dT)/aug-cc-pVTZ and experimental results.

Acknowledgments T. S. is grateful for the Research Fellowships from Japan Society for the Promotion of Science for Young Scientists (JSPS). This work has been supported by Grants-in-Aid for Scientific Research (KAKENHI) (Nos. 21550014, 19750046, 19350070) from JSPS and that on Grant-in-Aid for Scientific Research on Innovative Areas ("Coordination Programming" area 2170, No. 22108515) from the Ministry of Education, Culture, Sports, Science, and Technology (MEXT).

Appendix

Definitions of acronyms are given in Table 7.

Table 7 Acronyms used in the text

Acronym	Method
MRCC	Multireference coupled cluster
MkMRCCSD	Mukherjee's state-specific coupled cluster singles and doubles
HONO	Highest occupied natural orbital
LUNO	Lowest occupied natural orbital
UNO	UHF natural orbital
CNO	CASSCF natural orbital
ULO	UHF localized natural orbital
CLO	CASSCF localized natural orbital
RLO	ROHF localized molecular orbital
RMRCCSD	Reduced multireference coupled cluster singles and doubles
SS-EOM-CCSD[+*n*]	State-specific equation-of-motion coupled cluster singles and doubles. *n* more electrons in the vacuum state than in the final state of interest
EOM-SF-CC(2,3)	Equation-of-motion spin-flip coupled cluster. (2,3) denotes SD for the CC part and SDT for the excitation-energy part

Table 7 continued

Acronym	Method
4R BWCCSD it	Four reference Brillouin Wigner coupled cluster singles and doubles with an iterative size-extensivity correction
SU CCSD	State-universal coupled cluster singles and doubles
MRCISD	Multireference configuration interaction method with all singles and doubles
EOM-SF-CCSD(dT)	Equation-of-motion coupled cluster singles and doubles with perturbative triples corrections
MR-ACPF	Multireference averaged coupled-pair functional

References

1. Salem L (1982) Electrons in chemical reactions: first principles. Wiley, New York
2. Borden WT (1982) Diradicals. Wiley, New York
3. Dowd P (1966) J Am Chem Soc 88:2587
4. Chenier PJ (1978) J Chem Educ 55:286
5. Osamura Y, Borden WT, Morokuma K (1984) J Am Chem Soc 106:5112
6. Coolidge MB, Yamashita K, Morokuma K (1990) J Am Chem Soc 112:1751
7. Hirano T, Kumagai T, Miyashi T (1991) J Org Chem 56:1907
8. Wenthold PG, Hu J, Squires RR, Lineberger WC (1996) J Am Chem Soc 118:475
9. Wenthold PG, Lineberger WC (1999) Acc Chem Res 32:597
10. Cramer CJ, Smith BA (1996) J Phys Chem 100:9664
11. Schalley CA, Blanksby S, Harvey JN, Schröder D, Zummack W, Bowie JH, Schwarz H (1998) Eur J Org Chem 987–1009
12. Li J, Worthington SE, Cramer CJ (1998) J Chem Soc Perkin Trans 2:1045
13. Hess BA Jr, Eckart U, Fabian J (1998) J Am Chem Sco 120:12310
14. Brown EC, Borden WT (2002) J Phys Chem A 106:2963
15. Shipchenko LV, Krylov AI (2002) J Chem Phys 117:4694
16. Shipchenko LV, Krylov AI (2005) J Chem Phys 123:084107
17. Brabec J, Pittner J (2006) J Phys Chem A 110:11765
18. Harmata M (2006) Adv Synth Catal 348:2297
19. Demel O, Shamasundar KR, Kong L, Nooijen M (2008) J Phys Chem A 112:11895
20. Li X, Paldus J (2008) J Chem Phys 129:174101
21. Shen J, Fang T, Li S, Jiang Y (2008) J Phys Chem A 112:12518
22. Ichino T, Villano SM, Gianola AJ, Goebbert DJ, Velarde L, Sanov A, Blanksby SJ, Zhou X, Hrovat DA, Borden WT, Lineberger WC (2009) Angew Chem Int Ed 48:8509
23. Dong H, Hrovat DA, Quast H, Borden WT (2009) J Phys Chem A 113:895
24. Bettinger HF (2010) Angew Chem Int Ed 49:670 (doi:10.1002/anie.200905482 for the English version. doi:10.1002/ange.200905482 for the German version.)
25. Mozhayskiy V, Goebbert DJ, Velarde L, Sanov A, Krylov AI (2010) J Phys Chem A 114:6935
26. Carsky P, Paldus J, Pittner J (2010) Recent progress in coupled cluster methods: theory and applications (challenging and advances in computational chemistry and physics). Springer, New York
27. Raghavachari K, Trucks GW, Pople JA, Head-Gordon M (1989) Chem Phys Lett 157:479
28. Fukutome H (1968) Prog Theoret Phys 40:998
29. Hirao K (1992) Chem Phys Lett 190:374
30. Andersson K, Malmqvist P-A, Roos BO (1992) J Chem Phys 96:1218
31. Maranzana A, Ghigo G, Tonachini G (2000) J Am Chem Soc 122:1414
32. Park K, West A, Raheja E, Sellner B, Lischka H, Windus TL, Hase WL (2010) J Chem Phys 133:184306
33. West AC, Kretchmer JS, Sellner B, Park K, Hase WL, Lischka H, Windus TL (2009) J Phys Chem A 113:12663
34. Jeziorski B, Monkhorst HJ (1981) Phys Rev A 24:1668
35. Mukherjee D, Pal S (1989) Adv Quant Chem 20:292
36. Balkova A, Bartlett RJ (1994) J Chem Phys 101:8972
37. Mahapatra US, Datta B, Mukherjee D (1999) J Chem Phys 110:6171
38. Pittner J, Nachtigall P, Cársky P, Másik J, Hubac I (1999) J Chem Phys 110:10275
39. Evangelista FA, Allen WD, Schaefer HF III (2006) J Chem Phys 125:154113
40. Evangelista FA, Allen WD, Schaefer HF III (2007) J Chem Phys 127:024102
41. Bartlett RJ (1981) Ann Rev Phys 32:359
42. Szabo A, Ostlund NS (1996) Modern quantum chemistry. Dover, New York
43. Yamaguchi K, Fukui H, Fueno T (1986) Chem Lett 625–628
44. Yamaguchi K, Takahara Y, Fueno T (1986) In: Smith VH, Schaefer HF, Morokuma K (eds) Applied quantum chemistry, Boston, MA, US
45. Yamaguchi K, Takahara Y, Fueno T, Houk KN (1988) Theor Chim Acta 73:377
46. Purvis GD III, Bartlett RJ (1982) J Chem Phys 76:1910
47. Handy NC, Pople JA, Head-Gordon M, Raghavachari K, Trucks GW (1989) Chem Phys Lett 164:185
48. Nishihara S, Yamanaka S, Saito T, Kitagawa Y, Kawakami Y, Okumura M, Yamaguchi K (2010) Int J Quant Chem 110:3015
49. Nishihara S, Saito T, Yamanaka S, Kitagawa Y, Kawakami T, Okumura M, Yamaguchi K (2010) Mol Phys 108:2559
50. Saito T, Nishihara S, Yamanaka S, Kitagawa Y, Kawakami T, Okumura M, Yamaguchi K (2010) Mol Phys 108:2533
51. Saito T, Nishihara S, Kitagawa Y, Kawakami T, Yamanaka S, Okumura M, Yamaguchi K (2010) Chem Phys Lett 498:253
52. Purvis GD III, Sekino H, Bartlett RJ (1988) Collect Czech Chem Commun 53:2203
53. Yamaguchi K (1975) Chem Phys Lett 30:330
54. Yanai T, Tew D, Handy NC (2004) Chem Phys Lett 393:51
55. Dinning TH Jr (1989) J Chem Phys 90:1007
56. Becke AD (1988) Phys Rev A 38:3098
57. Lee C, Yang W, Parr RG (1988) Phys Rev B 37:785
58. Becke AD (1993) J Chem Phys 98:5648
59. Iikura H, Tsuneda T, Yanai T, Hirao K (2001) J Chem Phys 115:3540
60. Frisch MJ, Trucks GW, Schlegel HB, Scuseria GE, Robb MA, Cheeseman JR, Scalmani G, Barone V, Mennucci B, Petersson GA, Nakatsuji H, Caricato M, Li X, Hratchian HP, Izmaylov AF, Bloino J, Zheng G, Sonnenberg JL, Hada M, Ehara M, Toyota K, Fukuda R, Hasegawa J, Ishida M, Nakajima T, Honda Y, Kitao O, Nakai H, Vreven T, Montgomery JA Jr, Peralta JE, Ogliaro F, Bearpark M, Heyd JJ, Brothers E, Kudin KN, Staroverov VN, Kobayashi R, Normand J Raghavachari K, Rendell A, Burant JC, Iyengar SS, Tomasi J, Cossi M, Rega N, Millam NJ, Klene M, Knox JE, Cross JB, Bakken V, Adamo C, Jaramillo J, Gomperts R, Stratmann RE, Yazyev O, Austin AJ, Cammi R, Pomelli C, Ochterski JW, Martin RL, Morokuma K, Zakrzewski VG, Voth GA, Salvador P, Dannenberg JJ, Dapprich S, Daniels AD, Farkas

Ö, Foresman JB, Ortiz JV, Cioslowski J, Fox DJ (2009) Gaussian 09, Revision A.2. Gaussian, Inc., Wallingford
61. Schmidt MW, Baldridge KK, Boatz JA, Elbert ST, Gordon MS, Jensen JH, Koseki S, Matsunaga N, Nguyen KA, Su SJ, Windus TL, Dupuis M, Montgomery JA (1993) J Comput Chem 14:1347
62. Crawford TD, Sherrill CD, Valeev EF, Fermann JT, King RA, Leininger ML, Brown ST, Janssen CL, Sedil ET, Kenny JP, Allen WD (2007) J Comput Chem 28:1610
63. Li X, Paldus J (2009) J Chem Phys 131:114103
64. Kendall RA, Dunning TH Jr, Harrison RJ (1992) J Chem Phys 96:6796